Computational and Structural Biotechnology Journal 20 (2022) 1378–1388

COMPUTATIONAL AND STRUCTURAL BIOTECHNOLOGY JOURNAL

journal homepage: www.elsevier.com/locate/csbj

Understanding desaturation/hydroxylation activity of castor stearoyl Δ^9-Desaturase through rational mutagenesis

Michal Tupec [a], Martin Culka [a], Aleš Machara [a], Stanislav Macháček [a], Daniel Bím [a], Aleš Svatoš [a,b], Lubomír Rulíšek [a,*], Iva Pichová [a,*]

[a] Institute of Organic Chemistry and Biochemistry, Czech Academy of Sciences, Flemingovo nám. 2, Prague 16610, Czech Republic
[b] Max-Planck Institute for Chemical Ecology, Hans-Knöll-Straße 8, Jena 07745, Germany

ARTICLE INFO

Article history:
Received 12 January 2022
Received in revised form 11 March 2022
Accepted 11 March 2022
Available online 14 March 2022

Keywords:
Δ^9 desaturase
Methane monooxygenase
Reaction mechanism
Proton transfer
Desaturation
Hydroxylation

ABSTRACT

A recently proposed reaction mechanism of soluble Δ^9 desaturase (Δ^9D) allowed us to identify auxiliary residues His203, Asp101, Thr206 and Cys222 localized near the di-iron active site that are supposedly involved in the proton transfer (PT) to and from the active site. The PT, along with the electron transfer (ET), seems to be crucial for efficient desaturation. Thus, perturbing the major PT chains is expected to impair the native reaction and (potentially) amplify minor reaction channels, such as the substrate hydroxylation. To verify this hypothesis, we mutated the four residues mentioned above into their counterparts present in a soluble methane monooxygenase (sMMO), and determined the reaction products of mutants. We found that the mutations significantly promote residual monohydroxylation activities on stearoyl-CoA, often at the expense of native desaturation activity. The favored hydroxylation positions are C_9, followed by C_{10} and C_{11}. Reactions with unsaturated substrate, oleoyl-CoA, yield *erythro*-9,10-diol, *cis*-9,10-epoxide and a mixture of allylic alcohols. Additionally, using 9- and 11-hydroxystearoyl-CoA, we showed that the desaturation reaction can proceed only with the hydroxyl group at position C_{11}, whereas the hydroxylation reaction is possible in both cases, i.e. with hydroxyl at position C_9 or C_{11}. Despite the fact that the overall outcome of hydroxylation is rather modest and that it is mostly the desaturation/hydroxylation ratio that is affected, our results broaden understanding of the origin of chemo- and stereoselectivity of the Δ^9D and provide further insight into the catalytic action of the $NHFe_2$ enzymes.

1. Introduction

Mono- and binuclear non-heme iron (NHFe and $NHFe_2$, respectively) enzymes catalyze a multitude of C–H bond functionalizations in alkyl chains and aromatic rings, such as heterocyclic ring forming/opening, epoxidation, hydroxylation, aldehyde deformylation, or C–C bond desaturation [1–3]. One of the prominent examples of $NHFe_2$ enzymes is the soluble chloroplastic stearoyl-acyl carrier protein (ACP) Δ^9 desaturase (Δ^9D, EC 1.14.19.2, Pfam ID PF03405). The Δ^9D is an O_2-dependent enzyme that has evolved to convert stearoyl-ACP (18:ACP) to oleoyl-ACP (9*Z*-18:1ACP) as a part of the unsaturated fatty acid biosynthetic pathway in plants [4–8]. The process, which is highly chemo-, regio- and stereoselective, involves a *cis* double bond insertion into a C_9–C_{10} bond of the stearoyl chain via two sequential hydrogen atom abstraction (HAA) reactions [9–20].

To achieve the desired chemical transformation, Δ^9D employs several highly reactive iron-(per)oxo intermediates, starting with the spectroscopically characterized 1,2-μ-peroxo-$[Fe^{III}]_2$**P** intermediate (Fig. 1) [19]. The potential role of these intermediates in the Δ^9D catalytic mechanism was carefully investigated in recent quantum mechanics and molecular mechanics (QM/MM) and QM studies [21,22]. It has led to a formulation of the Δ^9D reaction mechanism which is, to a great extent, consistent with available experimental observations. Still, the calculations do not unambiguously explain how the enzyme promotes substrate desaturation at the expense of thermodynamically more favorable hydroxylation. Bím *et al.* have suggested that stearoyl-ACP desaturation is the result of a kinetic control that manages the delicate balance between several competing pathways [22].

According to QM/MM computations, desaturation largely hinges on the access of protons and electrons into the Fe_2 active

* Corresponding authors.
E-mail addresses: lubos@uochb.cas.cz (L. Rulíšek), iva.pichova@uochb.cas.cz (I. Pichová).

https://doi.org/10.1016/j.csbj.2022.03.010

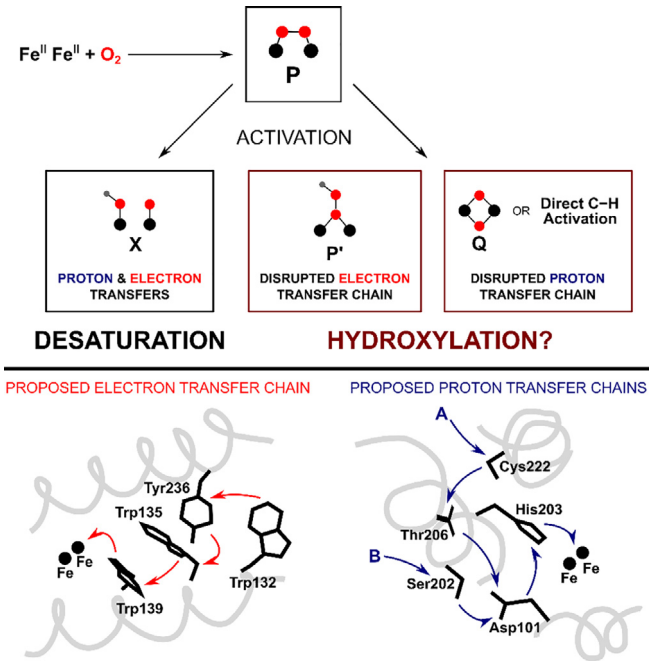

Fig. 1. Reactive intermediates and electron/proton transfer chains in Δ^9D. *Top*: Proposed catalytic pathways of Δ^9D [22]. Resting state of the wild-type Δ^9D is activated by O_2, leading to the formation of spectroscopically characterized, but unreactive, **P** intermediate (1,2-μ-peroxo-[Fe^{III}]$_2$). Activation of the **P** intermediate by electron and proton transfers was then proposed to generate mixed-valence '**X**' intermediate (Fe^{III}-OH, Fe^{IV}=O), capable of initial C–H activation ultimately leading to substrate desaturation. Alternative pathways were also investigated that do not necessitate electron or proton transfers; however, the rate-determining steps required significantly higher activation energies (**P'** and **Q** intermediates). Herein, we suggest that disruption of the electron and/or proton transfer chains by mutagenesis might thus open new reactive pathways, e.g., by modulating the tight balance between Δ^9D desaturation and hydroxylation reactivity. *Bottom*: The proposed electron (*left*) and proton (*right*) transfer chain residues are based on experiments dissecting the electron transfer in desaturase [51] and the sequence analysis of multiple $NHFe_2$ enzymes [22]. Note that two proton transfer chains (denoted as A and B) were suggested; in this work, we have introduced the mutations of Asp101, His203, Thr206 and Cys222 residues of the proton transfer chain A, which shares Asp101 and His203 with the proton transfer chain B.

site (Fig. 1). The initially formed **P** intermediate is proposed to be protonated and reduced to produce the reactive mixed-valent **X** intermediate (Fe^{III}-OH, Fe^{IV}=O), capable of substrate oxidation. Based on the mechanistic study [22] and $NHFe_2$ enzymes sequence analysis, the protonation is achieved through the iron-coordinating Glu105, to which a proton is shuttled by the neighboring His203 and a more distant chain of polar residues (Asp101, Thr206 and Cys222).

Counterparts of the soluble acyl-ACP desaturases – membrane fatty acyl-coenzyme A (CoA) desaturases (FADs) and FAD-like enzymes – are capable of (or even specialized to perform) various oxidations aside from desaturation, e.g. epoxidation, acetylenation and the allylic hydroxylation of a double bond [23–25] or the hydroxylation of a single bond [26,27]. However, the precise molecular mechanism behind the specificity shift from a presumably ancestral desaturation process remains enigmatic. The findings on similar reactions in soluble Δ^9Ds are limited to a few examples (Fig. 2). When presented with 9-fluorinated acyl-ACPs, the Δ^9D from *Ricinus communis* (*Rco*Δ^9D) hydroxylates at C_{10} and C_{11}, resulting in vicinal or methylene-bridged fluorohydrins (Fig. 2A) [28,29]. The same desaturase has been shown to oxidatively cleave 9- and 10-ethers, resulting in alcohol and aldehyde [30]. Additionally, it has been shown to oxidize 9- and 10-thia derivatives to respective sulfoxides or to induce oxidative cleavage into thiol and aldehyde (Fig. 2BC), the latter occurring only with 9-thia substrate [31]. The mutant *Rco*Δ^9D$^{T117R/G188L/D280K}$ converts Δ^9 unsaturated substrates to a series of allylic alcohols and a diene, with the hydroxyls being derived from dioxygen (Fig. 2D) [32]. Reaction of the same triple mutant with 9*Z*-18:1ACP (i.e. the native product of Δ^9D) yields 10*E*–9–OH–18:1 product and a lower amount of 10*Z* isomer, while the reaction with 9*E*-18:1ACP affords 10*Z*-9-OH-18:1, 10*E*-9-OH-18:1 and 9*E*-11-OH-18:1 products (the latter two present at lower quantity), along with 9*E*11*Z*–18:2ACP. In addition, when introduced individually, the mutations T117R and D280K (the latter to a lesser extent) confer dioxygenase specificity on the enzyme to form a saturated vicinal diol in *erythro*-9,10 configuration from 9*Z*-18:1ACP (Fig. 2D) [33]. Minor dihydroxylation and allylic hydroxylation activities have also been detected in the wild type Δ^9D after prolonged incubation. Nevertheless, the described mutations are somewhat distant from the active site. Their hydroxylation-inducing effect presumably originates from a modified positioning of the ACP or substrate fatty acyl chain in the enzyme cavity, and the hydroxylation reactions only occur on substrates which have been pre-oxidized by desaturation or other functionalization. To the best of our knowledge, there has been no example of a Δ^9D hydroxylating un-activated alkane chains in a single step.

Here, our aim is to exploit the practical consequences of the theoretically predicted Δ^9D reaction mechanism. Based on a comparison with a soluble methane monooxygenase (sMMO), i.e. structurally similar $NHFe_2$ enzyme hydroxylating methane to methanol in bacteria [34], we aim to devise a set of mutations in Δ^9D which may modulate its specificity and promote acyl chain hydroxylation, or possibly, other oxidation reactions. Modulating the enzyme specificity towards a different channel represents a route to potential biotechnological applications and, at the same time, it further extends our understanding of the mechanistic details of the $NHFe_2$ catalytic action.

2. Materials and methods

2.1. Materials

Spinach ferredoxin (Fd; >15 %, Sigma-Aldrich) and spinach ferredoxin–$NADP^+$ reductase (FdR; >15 U.mg^{-1}, Sigma-Aldrich) were dissolved in a storage buffer (200 g.L^{-1} glycerol, 0.15 M NaCl, 25 mM KH_2PO_4, pH 7.5) to a concentration of 0.4 mM and 20 U.mL^{-1}, respectively, and stored in aliquots at −80 °C. NADPH tetrasodium salt (Santa Cruz Biotechnology) and stearoyl-CoA (18:CoA) free acid (Carbosynth) were dissolved/suspended in 50 mM KH_2PO_4 buffer, pH 7.5, to a concentration of 40 mM and 10 mM, respectively, and were used immediately. ATP disodium salt (Sigma-Aldrich) and coenzyme A (CoA) tri-lithium salt (Megazyme) were dissolved in 100 mM K_2HPO_4 buffer, pH 7.5, to a concentration of 200 mM and 100 mM, respectively, and were used immediately. Chicken egg lysozyme (CEL) and cOmplete EDTA-free protease inhibitor cocktail (PIC) were purchased from Sigma-Aldrich; catalase from bovine liver (CAT; 245,000 U.mL^{-1}) was purchased from Fluka. The solvents used for extractions and chromatography were of HPLC or MS grade, and the other chemicals were of analytical grade.

Silylated and methylated standards 9-OTMS-18:Me, 10-OTMS-18:Me, 11-OTMS-18:Me and *erythro*-9,10-bisOTMS-18:Me were prepared from the respective free (di)hydroxy-acids by acid-catalyzed esterification using 2.5 %(v) H_2SO_4 in MeOH, followed by extraction/neutralization and silylation as described in section ***2.9.*** The standard of *threo*-9,10-bisOTMS-18:Me was prepared from its dihydroxy methyl ester by silylation. The standard of *trans*-9,10-epoxy-18:Me was prepared from 9*E*-18:1Me by epoxidation with *meta*-chloroperoxybenzoic acid.

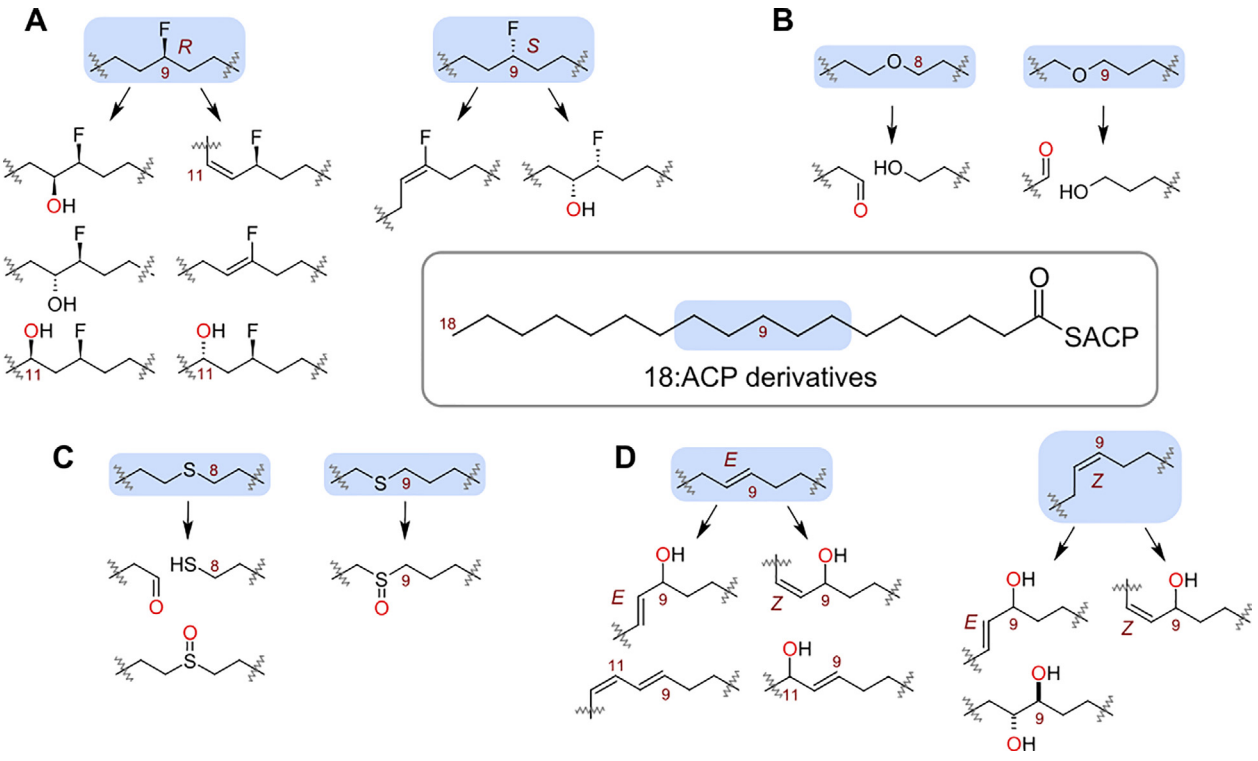

Fig. 2. Overview of Δ^9D-catalyzed non-canonical oxidative reactions reported in the literature [28–33]. Reactions with fluorinated (**A**), etheric (**B**), thioetheric (**C**) and olefinic (**D**) acyl-ACP substrates yield several oxidized products, including fluorohydrins, vinylfluorides, aldehydes, alcohols, sulfoxides, thiols, allylic alcohols, diols and dienes.

2.2. Organic synthesis

Details on the synthesis of modified fatty acids are provided in the Supporting Information.

2.3. Gene cloning and mutagenesis

The truncated region coding the amino acids P53–L396 of *Rco*Δ^9D (UniProtKB accession number P22337) and its two mutant forms *Rco*Δ^9D$^{D101I/H203I}$ and *Rco*Δ^9D$^{D101I/H203I/T206V/C222F}$ (numbering in mutants based on the mature protein sequence starting $A^1S^2T^3$-LKSG…) and the full region coding long-chain fatty acyl-CoA ligase from *E. coli* (*Eco*FadD; UniProtKB accession number P69451) were obtained by custom gene synthesis (GenScript). The genes were codon-optimized with a trade-off for both *E. coli* and *S. cerevisiae* (Δ^9Ds), or for *E. coli* (*Eco*FadD). Δ^9D and *Eco*FadD sequences were amplified from the shipping vector by PCR using Phusion high-fidelity DNA polymerase (New England Biolabs) with specific primers (Table S1 in the Supporting Information). They were cloned at the *Nde*I–*Bam*HI site of the pET-14b vector (Novagen) containing an *N*-terminal *hexa*-histidine tag and a thrombin cleavage site. Q5 high-fidelity DNA polymerase-mediated plasmid amplification using mutagenic primers (Table S1), coupled with *Dpn*I digestion, was employed for the generation of the single mutants *Rco*Δ^9D^{D101I} and *Rco*Δ^9D^{H203I} from the Δ^9D template. All final constructs were verified by Sanger sequencing (Eurofins Genomics).

2.4. Δ^9D expression and purification

Wild-type Δ^9D and its mutants were expressed in an *E. coli* Lemo21(DE3) strain [35] using 2.5 L Tunair baffled shake flasks (IBI Scientific) filled with 0.4 L auto-induction medium [36], composed of 15 g.L^{-1} yeast extract, 10 g.L^{-1} peptone, 10 g.L^{-1} glycerol, 2 g.L^{-1} D–lactose, 0.5 g.L^{-1} D–glucose, 100 mM KH_2PO_4, pH 7.5, 50 mM NaCl, 25 mM $(NH_4)_2SO_4$ and 3 mM $MgSO_4$. The culture (starting $OD_{600} \sim 0.01$) was supplemented with 100 mg.L^{-1} ampicillin, 30 mg.L^{-1} chloramphenicol, 20 µM $FeCl_3$ and 1 mM L–rhamnose, and shaken for 8 h at 37 °C, 250 RPM, and then shaken for further 16–20 h at 17 °C. The cells (yielding 15–30 g per liter of culture) were harvested by centrifugation and stored at −80 °C.

After thawing, the cells were suspended in 5 volumes of lysis buffer (100 g.L^{-1} glycerol, 0.5 M NaCl, 50 mM K_2HPO_4, pH 8.0, 20 mM imidazole) using a tissue homogenizer. Additionally, the suspension was supplemented with 5 mM β-mercaptoethanol (ME), 0.2 mg.mL^{-1} CEL and 1 tablet of PIC per ~30 g cells and incubated for 3 h at 4 °C while rolling. Cells were broken via 7 cycles of sonication, and the resulting crude lysate was clarified by centrifugation (30,000×*g*, 30 min). The supernatant was filtered through 0.6 µm pore glass fiber filter and pump-loaded onto HisTrap Fast Flow 5 mL column (Cytiva) using ÄKTA start chromatograph (Cytiva). The column was subsequently washed with 250 mL of wash buffer (0.35 M NaCl, 25 mM K_2HPO_4, pH 8.0, 5 mM ME, 20 mM imidazole), and the proteins were eluted by a two-step gradient of 5 mL of 25 % elution buffer (wash buffer with 200 mM imidazole) and 30 mL of 100 % elution buffer. The Δ^9D concentration was estimated using the calculated extinction coefficient of 56.4 mM^{-1}.cm^{-1} at 280 nm [37]. After being stored at −80 °C, the pooled fractions were concentrated using an Amicon Ultra-15 centrifugal filter (10 kDa cut–off, Merck) to ~5–15 mg.mL^{-1} in buffer S1 (0.35 M NaCl, 25 mM K_2HPO_4, pH 8.0, 5 mM ME), and then immediately injected onto HiLoad 16/600 Superdex 200 pg column (Cytiva), equilibrated to buffer S1, mounted to an ÄKTA pure chromatograph (Cytiva). The resulting Δ^9D fractions were concentrated to 0.4 mM (~17 mg.mL^{-1}; slight yellow-green color, overall yield ~20–40 mg protein per liter of culture) in buffer S1 containing 200 g.L^{-1} glycerol and stored in aliquots at −80 °C. The final proteins were analyzed by SDS-PAGE, followed by Coomassie brilliant blue staining.

2.5. EcoFadD expression and purification

The acyl-CoA ligase was expressed in Lemo21(DE3) and purified similarly to the procedure described above for Δ^9Ds. The auto-induction medium (0.5 L) contained 0.5 mM L–rhamnose and no $FeCl_3$. Cells were lysed in buffer (100 g.L^{-1} glycerol, 0.5 M NaCl, 50 mM K_2HPO_4, pH 8.0, 5 mM imidazole, 1 mM $MgSO_4$,), supplemented with 10 mM ME, 0.5 mg.mL^{-1} CEL, 1 tablet of PIC per ~30 g cells and 2 %(v/v) Tween 20 (the latter added 30 min before sonication). After loading the clarified lysate, a HisTrap FF 5 mL column was washed with 250 mL of wash buffer [50 g.L^{-1} glycerol, 0.5 M NaCl, 50 mM K_2HPO_4, pH 8.0, 10 mM imidazole, 5 mM ME, 1 mM $MgSO_4$, 0.02 %(v/v) Tween 20], and the proteins were eluted with elution buffer (wash buffer with 500 mM imidazole). The *Eco*FadD concentration was estimated using an extinction coefficient of 54 mM^{-1}.cm^{-1} at 280 nm [37]. The pooled *Eco*FadD fractions were concentrated to 0.15 mM (~12 mg.mL^{-1}) using a centrifugal filter (50 kDa cut–off) in buffer S2 [100 mM NaCl, 20 mM K_2HPO_4, pH 8.0, 5 mM ME, 1 mM $MgSO_4$, 0.01 %(v/v) Tween 20], supplemented with 20 %(v/v) glycerol and stored in aliquots at −80 °C.

2.6. Preparative enzymatic thioesterifications

The fatty acyl-CoA thioesters (except for 18:CoA) were prepared enzymatically using purified *Eco*FadD (6 μM) in a reaction mixture containing 100 mM K_2HPO_4, pH 7.5, 50 mM NaCl, 5 mM $MgSO_4$, 5 mM ME, 1 mM Triton X-100, 5 mM ATP, 2 mM CoA, and 2.5 mM fatty acid (oleic acid: 14.1 mg, 50 μmol; 9-hydroxyoctadecanoic acid: 9.2 mg, 30 μmol; 11-hydroxyoctadecanoic acid: 7.5 mg, 25 μmol). The reaction was incubated at 40 °C in a liquid scintillation vial (25 mL) placed inside a shaker (~120 RPM) for 6 h. After 3 h and 5 h, samples (10 μL) were taken and analyzed by HPLC (see section **2.7.**) to assess the extent of thioesterification. Ultimately, the reaction was stopped by adding acetonitrile (MeCN) at a 1:1(v/v) ratio, and the resulting suspension was clarified by centrifugation (5000×*g*, 2 min). The supernatant was lyophilized, and the remaining residue was dissolved/suspended in up to 1.2 mL 50 mM KH_2PO_4 buffer, pH 7.5. Occasionally, heating at 60 °C was required to further aid with solubilization.

After clarifying the solution by brief centrifugation (14,000×*g*), the mixture was injected manually through a 7125 valve (Rheodyne) onto a Luna C18(2) AXIA LC column (Phenomenex; 5 μm, 100 Å, 250 × 21.2 mm) equipped with a SecurityGuard PREP C18 pre-column (Phenomenex; 15 × 21.2 mm). The synthetic acyl–CoA was purified on an Alliance HPLC system (Waters; e2695 separation module, 2995 PDA detector, Fraction Collector III) using a gradient of 25 mM ammonium formate ($HCOONH_4$) (A) and MeCN (B) at 9 mL.min^{-1} as follows: 5 min at 5 % B, 5 % B to 100 % B in 50 min, 100 % B to 5 % B in 10 min, and 10 min at 5 % B. Analytes were detected at 210–400 nm. Fractions corresponding to the synthesized acyl-CoA were combined and lyophilized.

9*Z*-Octadec-9-enoyl-CoA (oleoyl-CoA, 9*Z*-18:1CoA; Figure S1): 4.2 mg (yield 8%); retention time (RT) 9.13 min; HR-MS (negative ESI) *m*/*z* calculated for $C_{39}H_{67}N_7O_{17}P_3S$ [M−H]$^-$ 1030.3532, found 1030.3521; GC–MS (methyl ester derivative) *m*/*z* 55 (100, 69 (48), 74 (42), 222 (6), 264 (10), **296** (2).

9-Hydroxyoctadecanoyl-CoA (9-OH-18:CoA; Figure S2): 12.9 mg (yield 40%); RT 8.05 min; HR-MS (negative ESI) *m*/*z* calculated for $C_{39}H_{69}N_7O_{18}P_3S$ [M−H]$^-$ 1048.3638, found 1048.3624; GC–MS (TMS methyl ester derivative) *m*/*z* 73 (100), 74 (20), 75 (41), **229** (42), **259** (43), 339 (4), 355 (2), 371 (1).

11-Hydroxyoctadecanoyl-CoA (11-OH-18:CoA; Figure S3): 3.6 mg (yield 14%); RT 8.12 min; HR-MS (negative ESI) *m*/*z* calculated for $C_{39}H_{69}N_7O_{18}P_3S$ [M−H]$^-$ 1048.3638, found 1048.3618; GC–MS (TMS methyl ester derivative) *m*/*z* 73 (100), 74 (27), 75 (44), **201** (57), **287** (35), 339 (4), 355 (1.5), 371 (1).

2.7. HPLC analysis

Analysis of *Eco*FadD-catalyzed reactions was performed on an UltiMate 3000 HPLC system (Thermo-Fisher). A sample of the reaction mixture was mixed with MeCN at a 1:1 (v/v) ratio, and after brief centrifugation (14,000×*g*), the supernatant was injected onto a Kinetex C18 column (Phenomenex; 5 μm, 100 Å, 150 × 4.6 mm) equipped with a SecurityGuard ULTRA C18 UHPLC pre–column (Phenomenex; 2 × 4.6 mm). The compounds were eluted using a gradient of 25 mM $HCOONH_4$ (A) and MeCN (B) at 1 mL.min^{-1} and 40 °C as follows: 1 min at 5 % B, 5 % B to 100 % B in 10 min, 100 % B to 5 % B in 3 min, and 2 min at 5 % B. Analytes were detected at 260 nm.

2.8. Desaturase assay

The desaturation and oxygenation activity of Δ^9Ds was assessed by incubating a particular enzyme (10 μM) in a 200 μL reaction mixture containing 0.15 M NaCl, 25 mM KH_2PO_4, pH 7.5, 4 μM Fd, 0.2 U.mL^{-1} FdR, 2 mM NADPH, 0.5 mM acyl-CoA, 1000 U.mL^{-1} CAT, 0.5 mM Triton X-100 and 10 g.L^{-1} glycerol [38–40]. The reaction was carried out in an open vial (1.5 mL) placed into a water bath at 35 °C for 4 h, and the mixture was subsequently lyophilized overnight to remove excess water.

2.9. Fatty acyl derivatization

The lyophilized Δ^9D reaction mixtures were subjected to base-catalyzed transesterification using 0.2 mL 1 M sodium methoxide suspension in MeOH. The reaction was incubated and shaken for 30 min, after which the methyl esters were extracted into 800 μL of hexane by vigorous mixing. The base was neutralized by adding 400 μL 0.25 M KH_2PO_4, 0.25 M Na_2HPO_4, pH 7, and 25 μL 4 M HCl. Approximately 750 μL of the upper hexane layer was transferred into a clean vial and a drop of ~0.6 M trimethylsilyldiazomethane in hexane was added to further methylate the unreacted acids. The mixture was incubated for 20 min and subsequently evaporated to dryness using nitrogen flow at 45 °C. Additionally, the free hydroxyls were silylated by adding 20 μL *N*,*O*-bis(trimethylsilyl)trifluoroacetamide and trimethylchlorosilane 99:1 mixture (TCI Europe) and 40 μL MeCN, and heating the mixture for 20 min at 70 °C. The silylating agent was then evaporated under nitrogen flow at 45 °C. The resulting fatty acyl derivatives were dissolved in 25 μL of hexane, the extract was then transferred into 0.1 mL vial insert, and stored at −20 °C before analysis.

2.10. GC×GC–MS analysis

Comprehensive two-dimensional gas chromatography-mass spectrometry (GC×GC–MS) was used for the analysis of derivatized Δ^9D–catalyzed reaction components. Separation was achieved on a non-polar primary column Rxi-5Sil MS (30 m, ID 250 μm, film thickness 0.25 μm, Restek) connected to a more polar secondary column Rxi-17Sil MS (1.4 m, ID 150 μm, film thickness 0.15 μm, Restek) on 6890 N gas chromatograph (Agilent Technologies) coupled to a Pegasus IV D TOF mass detector (LECO Corp.). The programmed run parameters were as follows: injector temperature 250 °C; column flow 1 mL.min^{-1} (helium); modulation period 4 s (hot pulse time 0.8 s, cool time 1.2 s); secondary oven temperature offset +10 °C relative to the primary oven; modulator temperature offset +20 °C relative to the secondary oven; primary oven temperature gradient: first ramp from 200 °C to 260 °C at 4 °C.min^{-1}; second ramp to 330 °C (hold 1 min) at 20 °C.min^{-1}; transfer line

temperature 260 °C; electron voltage −70 V; ion source temperature 220 °C; detector voltage 1500 V.

The C18 acyl derivatives were identified based on a comparison of their retention times and mass spectra with those of synthetic standards and spectra in libraries and/or in the literature. The quantitative data are represented either as a relative abundance (the percentage of a particular C18 product originating from the initial substrate, e.g. 18:CoA, at the end of a reaction) from total ion chromatogram, or as a peak area from extracted ion chromatogram at specified mass to charge (m/z). All quantifications were performed using four to six replicates (indicated as N). The results are reported as mean value ± S.D., including individual data points. Significance testing was performed by one-way analysis of variance and *post hoc* Tukey's honestly significant difference test.

2.11. Accession codes

The protein coding sequences of Δ^9D and its variants characterized in this study were deposited into GenBank (accession numbers MW460899–MW460903).

3. Results and discussion

3.1. Synthetic strategies towards oxidized fatty acids

Methyl *erythro*- and *threo*-9,10-dihydroxystearates (*erythro*/*threo*-9,10-bisOH-18:Me) as well as methyl *cis*–9,10–epoxystearate (*cis*-9,10-epoxy-18:Me) were prepared according to published procedures (Scheme S1 in the Supporting Information) [41,42]. The synthesis of 9-, 10- and 11–hydroxystearic acids was based on a modular method starting from corresponding ω-hydroxyalkanoic acids (Schemes S2–S4). They were converted to ω-aldehydes which were treated with Grignard reagents, providing C18 alkyl chains. The esters 9*Z*-11-OH-18:1Me and 9-OH-10*Z*-18:1Me were prepared in a similar manner (Schemes S5 and S6) [32]. At first, additions of lithium acetylides to corresponding aldehydes yielded hydroxyoctadecynoates that were partially hydrogenated over Lindlar catalyst to provide isomeric *Z*-allylalcohols. The synthesis of esters 9*E*-11-OH-18:1Me and 9-OH-10*E*-18:1Me was inspired by Weedon's communication [43]. In this approach, *Z*-allylalcohols, whose preparation was discussed above, were selectively oxidized with pyridinium chlorochromate to corresponding enones with an *E*-configuration. The subsequent selective transformation of the keto moiety by Luche reduction gave the required methyl esters. The synthetic procedures for all the products and their intermediates along with the NMR spectra are provided in the Supporting Information.

3.2. Rational design of Δ^9D mutants

Two proton transfer chains in Δ^9D were proposed in reference [22]: (A) His203, Asp101, Thr206, and Cys222; and (B) His203, Asp101, and Ser202 (*cf.* Fig. 1). The residues are evolutionarily conserved in plants and partially also in bacteria, and are thus natural candidates to be mutated in Δ^9D. Trusting the robustness of enzyme evolution, we did not expect to completely shut off the native reaction. However, any observable promotion of other reaction channels could provide a rationale for the postulated reaction mechanism and deepen our insight into $NHFe_2$ reactivity.

Based on the structural comparison of the active sites of Δ^9D (PDB ID 1AFR) and sMMO (PDB ID 1MHY), we designed a series of Δ^9D mutants where key residues involved in the proton transfer to the Δ^9D active site were replaced by hydrophobic residues present at equivalent positions in the sMMO hydroxylase (Fig. 3). In this way, we attempted to disrupt both proton transfer chains in

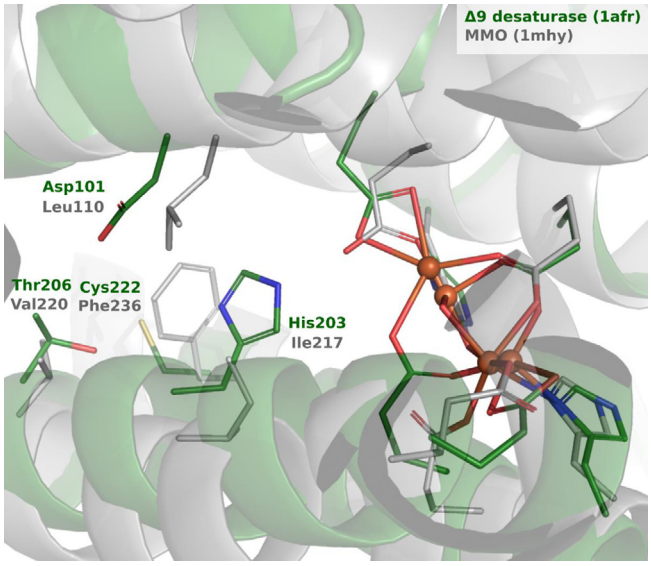

Fig. 3. Superposition of the Δ^9D (*green*) and sMMO (*gray*) active sites with the mutated residues highlighted. (For interpretation of the references to color in this figure legend, the reader is referred to the web version of this article.)

Δ^9D and thus divert the canonical **X** intermediate formation which could instead result in some alternative reactive intermediate promoting an alternative substrate activation; e.g., some sMMO **Q** intermediate analogue. We constructed two single mutants of the most proximal residues His203 (Δ^9D^{H203I}) and Asp101 (Δ^9D^{D101L}) which are critical for both of the proposed protonation transfer mechanisms, a double mutant of both residues ($\Delta^9D^{D101I/H203I}$) and a quadruple mutant of the whole proton transfer chain A ($\Delta^9D^{D101I/H203I/T206V/C222F}$). The sequence for Δ^9D cloning and heterologous expression was designed based on an *Rco*Δ^9D protein structure [44].

3.3. Δ^9D and its mutants hydroxylate the stearoyl chain

The wild type and mutated Δ^9Ds were expressed in *E. coli* and purified by affinity and gel chromatography (Figure S4 in Supporting Information). As substrates for the functional characterization, we used fatty acyl-CoAs [38] because of their commercial availability and simplicity of preparation. Based on the reported slower reaction rate with 18:CoA compared to 18:ACP [38,45], we prolonged the incubation times up to 4 h. For the identification of novel oxidation products in reaction mixtures, we employed comprehensive two-dimensional gas chromatography coupled with -mass spectrometry (GC×GC–MS) and a combination of transesterification/silylation (i.e. resulting in methyl esters and silylated methyl esters) to increase the sensitivity towards hydroxylated analytes [32,46].

Upon incubation with 18:CoA, which is an analogue of the native substrate 18:ACP, a major unsaturated product 9*Z*-18:1Me (Figure S5, molecular ion at m/z 296) was readily detected in the derivatized reaction mixtures of both Δ^9D and the mutants (Figure S6). The relative proportion of 18:CoA desaturated to 9*Z*-18:1CoA was similar for the wild type enzyme and both single mutants Δ^9D^{D101I} and Δ^9D^{H203I}, but it gradually decreased with multiple introduced mutations in $\Delta^9D^{D101I/H203I}$ and $\Delta^9D^{D101I/H203I/T206V/C222F}$ (Fig. 4A; $p < 0.01$).

In addition to the oleoyl-CoA product, we also noticed the appearance of minute amounts of what appeared to be monohydroxylated analytes in the derivatized reaction mixtures of all enzymes (Fig. 4BC). The fragmentation patterns of trimethylsilyl

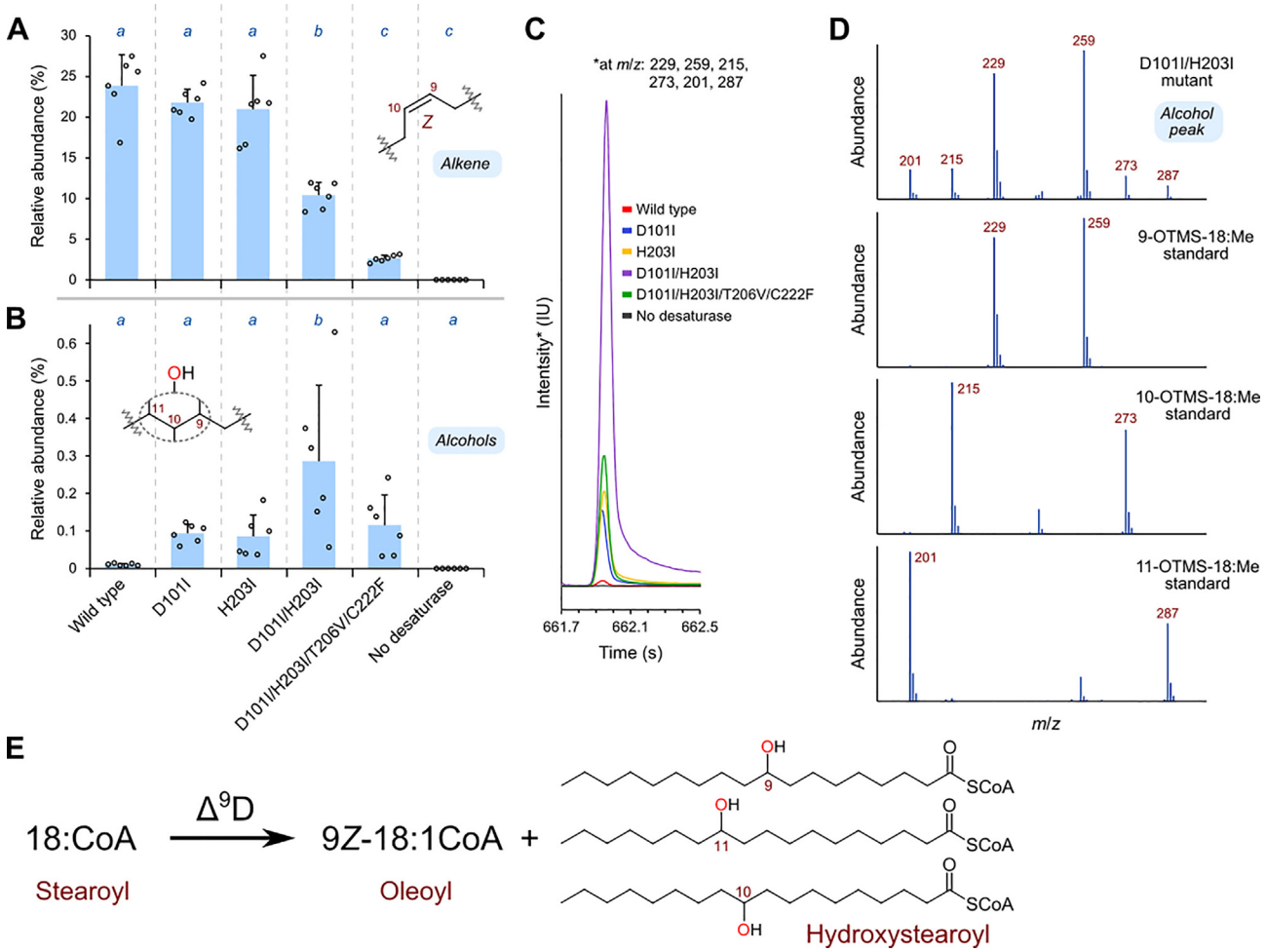

Fig. 4. GC×GC–MS analysis of desaturase reactions with stearoyl-CoA substrate after derivatization. (**AB**) The relative abundances (see section ***2.10.***) of oleate (**A**) as the expected Δ^9D product and a mixture of hydroxystearates (**B**) as novel minor products. The means sharing identical italicized letter are not significantly different from each other (see section ***2.10.***, $N = 6$; **A**: $p < 0.01$; **B**: $p < 0.05$). (**C**) A section of extracted chromatograms highlighting the relative amounts of enzymatically produced mixture of 9-, 10- and 11-hydroxystearates (extracted at *m*/*z* 229, 259, 215, 273, 201, 287). (**D**) Sections of mass spectra (*m*/*z* 190–300) of hydroxystearates obtained from a derivatized reaction mixture of $\Delta^9D^{D101I/H203I}$ and of synthetic standards 9-OTMS-18:Me, 10-OTMS-18:Me and 11-OTMS-18:Me. (**E**) A proposed reaction scheme for desaturase-catalyzed desaturation/hydroxylation.

(TMS) derivatives enabled us to identify them as a co-eluting mixture of methyl 9-(trimethysilyloxy)stearate (9-OTMS-18:Me), 10-OTMS-18:Me and 11-OTMS-18:Me, with diagnostic fragment ions at *m*/*z* 229 + 259, *m*/*z* 215 + 273, and *m*/*z* 201 + 287, respectively (Fig. 4D and Figure S7). Δ^9D and all four studied mutants preferentially hydroxylate at C_9, followed by hydroxylation at C_{10} and C_{11} (Figure S8). This preference for oxidation at C_9 is in contrast to the previous study where the products of oxidation at C_9 were not detected [30]. In this study, the substrate underwent a register shift to C_{11} instead (Fig. 2B) [30], but this may be due to the different nature of the non-native ether substrates that were used. The reaction mixture of the wild type enzyme also contained about 0.01% of hydroxylated fatty acyls, but the introduction of mutations increased their concentration, with the highest content up to 0.3% for mutant $\Delta^9D^{D101I/H203I}$ (i.e. approximately 30-fold *relative* increase). The very low production of hydroxylated acyls in the wild type enzyme is consistent with the previous work in which the authors did not detect any hydroxystearoyl products above the level of 0.1% [29]. Taking into consideration the apparent enzyme efficiency, i.e. native desaturation rate (Fig. 4A), a more profound effect of multiple introduced mutations on the hydroxylation process can be observed (Figure S9). The mutants $\Delta^9D^{D101I/H203I}$ and $\Delta^9D^{D101I/H203I/T206V/C222F}$ had the highest hydroxylation to desaturation ratio of 3–5% of the native reaction. On the other hand, the wild type Δ^9D had a hydroxylation to desaturation ratio at the significantly lower level of 0.04% ($p < 0.01$). Additionally, using the fragmentation patterns for TMS ethers [46], we detected more species of monohydroxylated analytes with the hydroxyl position varying from C_{12} to C_{17} (Figure S10). However, due to the lack of synthetic standards to unambiguously compare the retention and MS fragmentations and trace level quantities of these products connected with irreproducibility, we did not quantify these species. Similar hydroxylated C18 analytes (hydroxyl group at C_6 to C_{16}) of various origins have been detected at low abundance in animal tissues [47,48].

Possible subsequent reactions in which one of the primary products, unsaturated or hydroxylated acyl-CoA (Fig. 4E), acts as a new substrate for the desaturase are discussed further.

3.4. Reactions with non-native substrates afford variety of oxygenated species

Apart from the derivatives of oleoyl- and hydroxystearoyl-CoA products, we found several other oxygenated species in the 18:CoA reaction mixtures (*data not shown*), tentatively identified as diols, epoxides and allylic alcohols. The formation of vicinal diols and allylic alcohols has been reported in both wild type and mutant Δ^9D as a result of desaturase-catalyzed oxidation of 9*Z*-

18:1ACP [32,33], but not of the native 18:ACP. Therefore, we expected the same origin of these compounds when using CoA analogues of the acyl-ACPs. We proceeded with the reactions using 9*Z*-18:1CoA as a substrate, which we had prepared enzymatically from oleic acid using bacterial acyl-CoA ligase (*Eco*FadD).

Indeed, the previously reported vicinal diols and allylic alcohols, along with epoxides, are detectable in the derivatized reaction mixtures of all Δ^9D mutants upon incubation with the 9*Z*-unsaturated substrate. Methyl *erythro*-9,10-bis(trimethylsilyloxy) stearate (*erythro*-9,10-bisOTMS-18:Me) was present at up to 0.5% in the reaction mixtures (Fig. 5AB, Figure S11). The relative quantities followed the trend of desaturation efficiency to some extent (Fig. 4A), with the exception of both single mutants Δ^9D^{D101I} and Δ^9D^{H203I}, which dihydroxylated the substrate at a slightly higher rate than the wild type enzyme ($p < 0.05$). In the case of epoxides, methyl *cis*-9,10-epoxystearate (*cis*-9,10-epoxy-18:Me) could be detected in all derivatized reaction mixtures (Fig. 5CD and Figure S12). The *cis*–epoxide was the most abundant in Δ^9D^{D101I} at the level of 0.1%, followed by a decreased level in the remaining mutants. A low concentration of *cis*-epoxide below 0.02% was detected in the wild type enzyme, which is in agreement with previously published work stating that epoxides could not be detected in a Δ^9D reaction (below 0.5%) [32]. When we assessed the levels of the *threo*-9,10 isomer of diol, we found its overall production at least one-fold lower than that of *erythro*-9,10, and to a high extent, similar to that of *cis*–epoxide (Figure S13A and Fig. 5C). This may be a result of a non-enzymatic epoxide opening, with water acting as a nucleophile. The other epoxide isomer, *trans*-9,10-epoxy-18:Me, also presumably originates from a non-enzymatic reaction, as there is no large difference among the mixtures with enzymes and without enzymes, and its quantity falls below 0.025% (Figure S13B). We also detected multiple oxygenated products in the negative control (Fig. 5ACE, Figure S13), i.e. the reaction mixtures without added desaturases. It has been shown that unsaturated fatty acyls can undergo spontaneous (non-enzymatic) oxidations upon exposure to air, affording hydroperoxides, epoxides, diols and allylic alcohols [43,49,50].

Interestingly, we found two co-eluting mixtures of products which are both unsaturated and hydroxylated in the reactions mixtures (Figure S14). The products contain an allylic system based on the presence of *m*/*z* 129 from (trimethylsilyloxy)allyl ion (Figure S15 and Figure S16) and *m*/*z* 227/285 or *m*/*z* 241/271 from

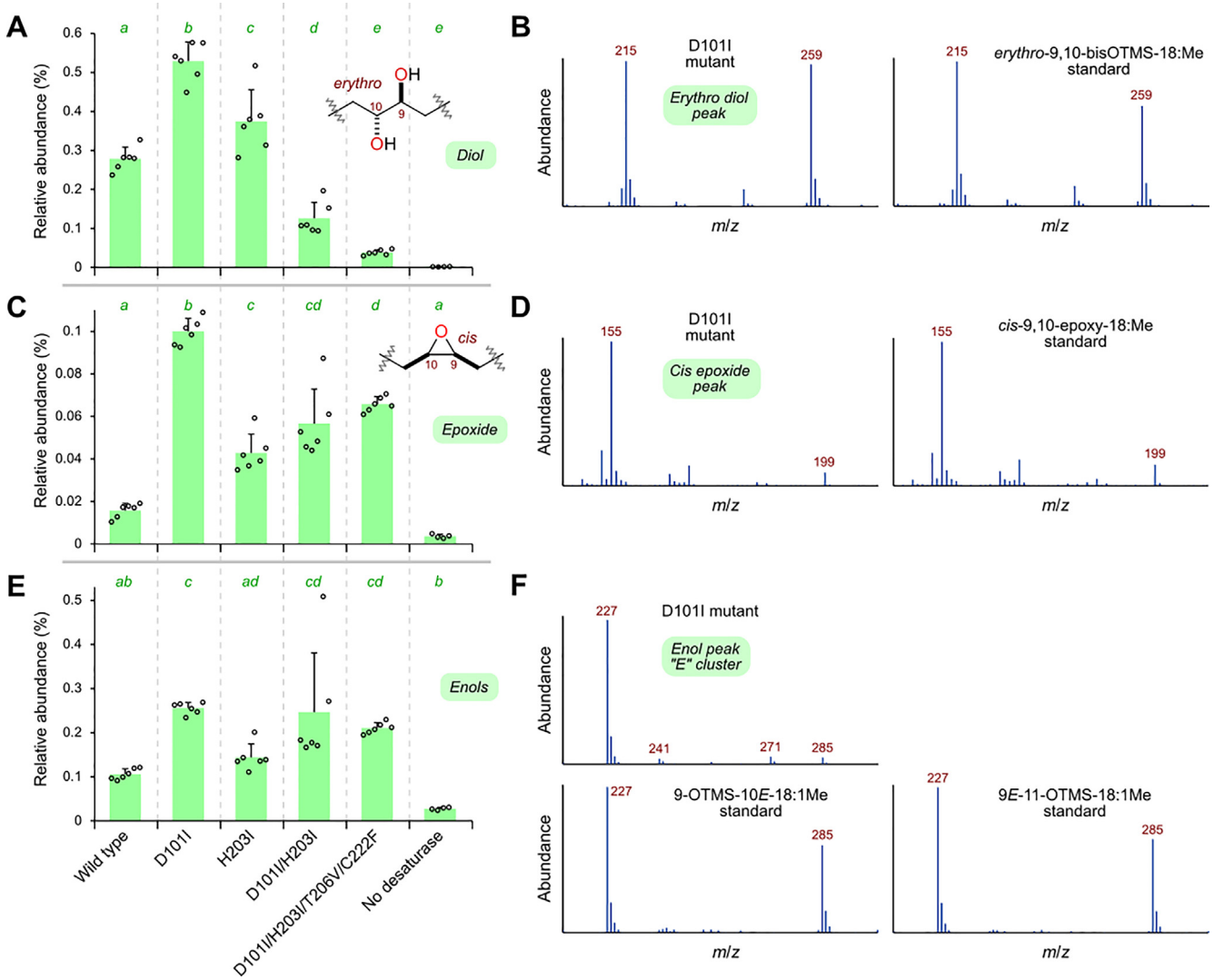

Fig. 5. GC×GC–MS analysis of desaturase reactions with oleoyl-CoA after derivatization. (**ACE**) The relative abundances (see section ***2.10.***) of *erythro*-9,10-dihydroxystearate (**A**), *cis*-9,10-epoxystearate (**C**) and a mixture of *E*-allylic hydroxyoctadecenoates (**E**). The means sharing an identical italicized letter are not significantly different from each other (see section ***2.10.***, $N = 6$, $N = 4$ for control; **A**: $p < 0.05$, **B**: $p < 0.01$, **C**: $p < 0.05$). (**BDF**) Sections of mass spectra obtained from a derivatized reaction mixture of Δ^9D^{D101I} and from synthetic standards *erythro*-9,10-bisOTMS-18:Me (**B**, *m*/*z* 200–275), *cis*-9,10-epoxy-18:Me (**D**, *m*/*z* 145–210), and 9-OTMS-10*E*-18:1Me and 9*E*-11-OTMS-18:1Me (**F**, *m*/*z* 215–300).

fragmentations on both sides of the allylic system (Fig. 5F and Figure S17). The 9–11 allylic system (*m/z* 227/285) was more abundant than the 8–10 system (*m/z* 241/271; Figure S14), and the *E* configuration of the double bond was more abundant than the *Z* configuration (Fig. 5E, and Figures S12C and S13). Because the *E* and *Z* derivatives of both 9–11 and 8–10 allylic systems co-elute, their spectra can be indistinguishable (Figure S15 and Figure S16), and because allylic alcohols can isomerize during the MS analysis [43], we quantified them as a mixture. The relative abundances of both *E* and *Z* isomers resembled the profile in *cis*-epoxide (Fig. 5E, Figure S13C), i.e. higher in mutants than in the wild type Δ^9D, ranging from 0.1% to 0.25% for *E* isomers and from 0.025% to 0.075% for *Z* isomers. We did not dissect the precise isomer composition of the co-eluting allylic alcohol peaks. These could essentially contain both 9-OH-10-ene / 9-ene-11-OH and 8-OH-9-ene / 8-ene-10-OH moieties (Figure S17). Allylic 9-OH-10*E*-18:1, 9-OH-10*Z*-18:1 and 9*E*-11-OH-18:1 have been already detected in Δ^9D reaction mixtures [32,33].

To further investigate the possible reversed order of the consecutive reactions, i.e. whether the substrate can be first hydroxylated and then desaturated by the enzyme, we synthetized two alcohol substrates by employing *Eco*FadD-catalyzed *in vitro* thioesterification. We chose 9–hydroxystearoyl-CoA (9-OH-18:CoA) as a probe for the formation of 9-OH-10-ene or 9,10-diol products, and 11-OH-18:CoA as a probe for the formation of 9-ene-11-OH product. Unlike in the case of a double bond, we did not expect any migration of the present hydroxyl group during the reaction.

When using 9-OH-18:CoA as a substrate, we detected diols and allylic alcohols in the derivatized reaction mixtures (Figure S18). The most abundant product was *erythro*-9,10-bisOTMS-18:Me (Fig. 6A), which is similar to reactions with 9*Z*-18:1CoA, and its relative quantity among the enzymes followed the trend of native desaturation efficiency (Fig. 4A). The other diol, *threo*-9,10-bisOTMS-18:Me, was present at a notably lower level (Figure S19A), most prominently in the Δ^9D^{H203I} mutant. On the other hand, the analysis of derivatized allylic alcohols

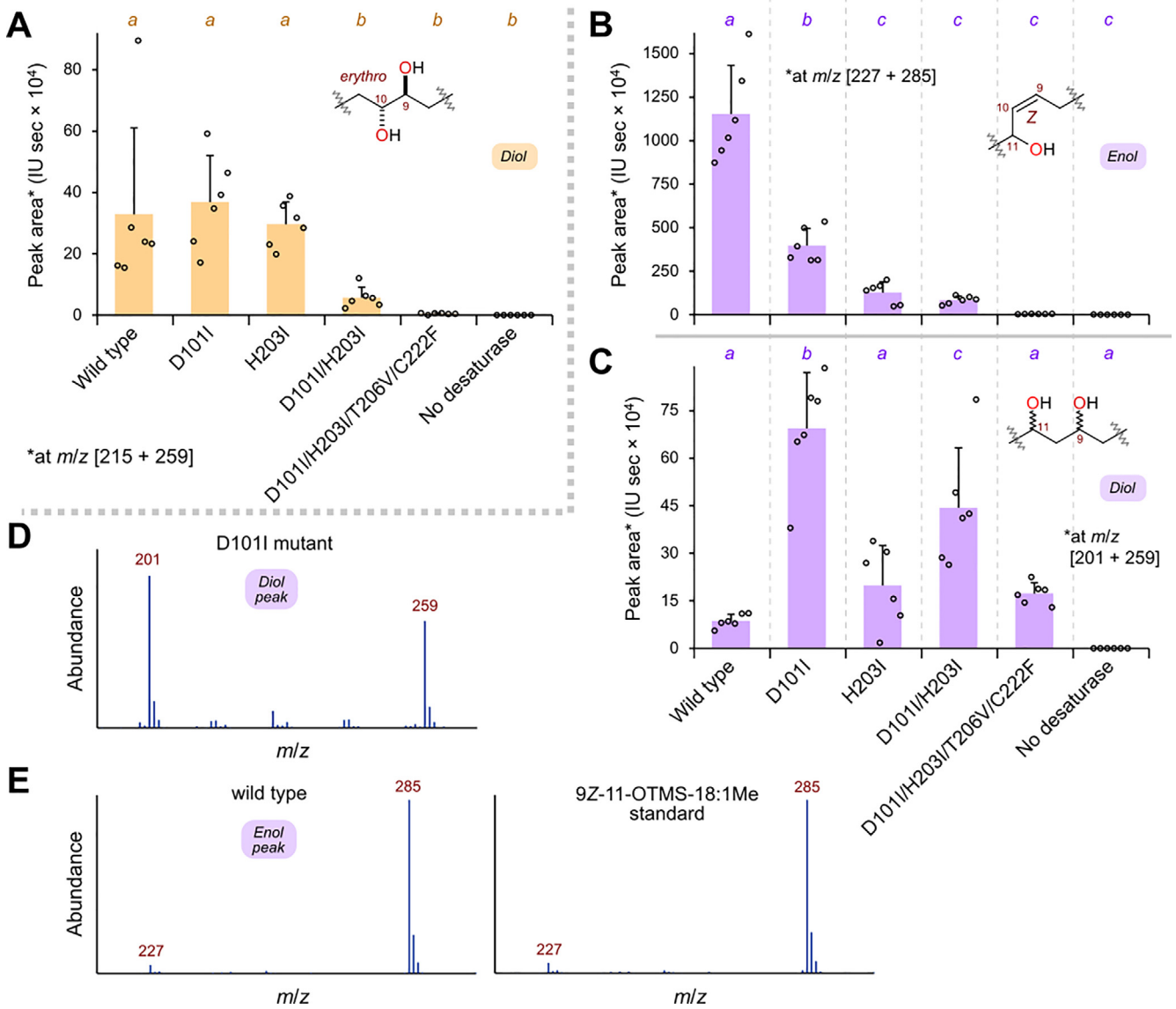

Fig. 6. GC×GC–MS analysis of desaturase reactions with 9- (*yellow*) and 11-hydroxystearoyl-CoA (*lila*) after derivatization. (**A**–**C**) The relative abundances (see section ***2.10.***) of *erythro*-9,10-dihydroxystearate (**A**), 11-hydroxyoleate (**B**) and diastereomer 1 of 9,11-dihydroxystearate (**C**). The means sharing identical italicized letter are not significantly different from each other (see section ***2.10.***, $N = 6$; **A**: $p < 0.05$, **B**: $p < 0.01$, **C**: $p < 0.05$). (**D**–**E**) Sections of mass spectra obtained from a derivatized reaction mixture of Δ^9D^{D101I} (**D**, substrate 11-OH-18:CoA, *m/z* 190–270), and from a derivatized reaction mixture of Δ^9D (substrate 11-OH-18:CoA, *m/z* 215–300) and a synthetic standard 9*Z*-11-OTMS-18:1Me (**E**). (For interpretation of the references to color in this figure legend, the reader is referred to the web version of this article.)

(9–OTMS-10*Z*/*E*-18:1Me) more likely points to a non-enzymatic origin or substrate contamination rather than a desaturase-catalyzed reaction, based on the very low differences from the negative control (Figure S19BC). This could mean that Δ^9D cannot easily dehydrate the substrate with the hydroxyl group present at the position where the native reaction occurs (i.e. at positions C_9 and C_{10}). Since the hydroxylation is favored thermodynamically, the balance between hydroxylation and desaturation must indeed be deliberately regulated by the kinetic step preceding any hydroxyl radical rebound mechanism.

Reactions with the artificial substrate 11-OH-18:CoA yielded an allylic alcohol and two diols (Figure S20). The allylic alcohol derivative, 9*Z*-11-OTMS-18:1Me, was easily identified by *m*/*z* 285 (Fig. 6E and Figure S20) and was present at high level in wild type Δ^9D (Fig. 6B); Δ^9D^{D101I}. The rest of the mutants showed gradually lower production of 9*Z*-11-OTMS-18:1Me. Our observations suggest that the desaturase can perform desaturation on a substrate with a hydroxyl group adjacent to the native desaturation positions C_9 and C_{10}. Additionally, we detected a new type of diastereomeric dihydroxy derivative in the reaction mixtures (Figure S20), assigned as 9,11-diols because of the presence of diagnostic fragment ions at *m*/*z* 201 and 259 (Fig. 6D and Figure S20). Their levels are almost identical (Fig. 6C and Figure S19D); most of this product is found in Δ^9D^{D101I} and $\Delta^9D^{D101I/H203I}$.

3.5. Modified reactivity of Δ^9D mutants is consistent with the proposed theoretical reaction mechanism

The wild-type Δ^9D was demonstrated to selectively desaturate the stearoyl-CoA substrate, with only insignificant amounts of the oxygenated species present in the derivatized reaction mixture (below 0.5%). Desaturation activity was not significantly altered by introducing single-point mutations (D101I and H203I); however, the double mutation (D101I/H203I) and the quadruple mutation (D101I/H203I/T206V/C222F) resulted in an approx. 2-fold and 9-fold decrease, respectively (Fig. 4A). By following the idea that Asp101, His203, Thr206, and Cys222 residues are involved in the proton transfer to/from the active site, the quadruple mutant should have the proton transfer chain A completely shut off (Fig. 1). However, a reduction but not a complete loss of desaturation suggests that an alternative protonation pathway can take over in Δ^9D and recover the formation of the reactive **X** intermediate. For instance, the second proton transfer chain (B chain in Fig. 1) was speculated to be operational [22], which has been only partially investigated in the present-study mutagenic experiments (although the mutated Asp101 and His203 most proximal to the active center are part of both chains). Notably, the Δ^9D active site is also relatively close to the protein/water interface, and thus the protons can be acquired directly from solvent, albeit with a presumably higher barrier. The switch toward a less energetically favorable proton delivery pathway is consistent with the gradual decrease in the Δ^9D desaturation activity. Therefore, this scenario is more likely than if the enzyme switched to another reaction mechanism that would compete with the canonical **P** → **X** intermediate transformation.

Besides reduced desaturation activity, we observed up to ~30-fold enhancement in the concentration of the monohydroxylated fatty acyls in reaction mixtures of the double and quadruple mutants (Fig. 4B). As expected, the hydroxylation pathway competes when the stearoyl-ACP desaturation activation energy is increased. However, the fact that we were unable to completely switch the chemoselectivity of Δ^9D suggests that desaturation and hydroxylation proceed through the same (possibly **X**) intermediate, whereas the products distribution is dictated by the relative energies of their rate-determining steps at some branching point along the reaction coordinate. The higher energy of the Glu105 protonation and/or Glu105 → FeO proton transfer likely affects both reaction pathways similarly, but it can co-influence the already close balance between desaturation and hydroxylation reactivity. Importantly, the results are consistent with the reaction mechanism that involves two separate reaction channels for desaturation and hydroxylation, i.e., without a possibility of dehydration of oxygenated-substrate intermediate. The provided experiments have thus considerably broadened our understanding of the initial theoretical Δ^9D reaction mechanism.

4. Conclusions

Using a set of rationally devised mutations of the second-sphere residues in the soluble Δ^9D, which are not directly involved in the reaction mechanism, we investigated the effects of proton transfer chains adjacent to the di-iron active site on the reaction outcome. Four residues – His203, Asp101, Thr206 and Cys222 – were mutated in a series of two single mutants, one double and one quadruple mutant, into their counterparts in the soluble MMO. Multiple mutations suppressed the native desaturation channel to some extent and promoted a hydroxylation channel, resulting in a mixture of alcohol products with preferred hydroxyl positions at C_9, C_{10} and C_{11}. It implies that, in accordance with the recently proposed reaction mechanism [22], the above-mentioned residues are efficient proton shuttles. Expectedly, due to the presence of other protic residues and solvent molecules, the enzyme has many ways to circumvent a break in the proton transfer chain (e.g. Ser202 residue, not investigated here, can be part of the second PT channel). However, this comes at the expense of a considerable loss of activity. In absolute numbers (i.e. conversion of the substrate), the hydroxylation is still a minor reaction channel in mutants (<1%), but the desaturation/hydroxylation ratio remarkably changes by a factor of up to 100 in mutants compared to the wild type.

In addition, the studied mutants produced overall increased levels of other oxidized products when incubated with non-native substrates. Upon reaction with oleoyl-CoA, we observed mainly *erythro*-9,10-diol accompanied by *cis*-9,10-epoxide and a mixture of allylic alcohols with a preference for an *E* configuration. Using 9-hydroxystearoyl-CoA as a substrate, we showed the desaturase is capable of carrying out hydroxylation at C_{10}, i.e. adjacent to the already present hydroxyl moiety. By employing 11-hydroxystearoyl-CoA as another oxidized substrate, a desaturation reaction was also possible, yielding 9*Z*-11-hydroxy allylic alcohol along with 9,11-diol products, the latter being hydroxylated at position C_9.

Combining experiments and theory, the findings reported herein have broadened our understanding of the catalytic action of the Δ^9D and other related $NHFe_2$ enzymes. It seems that their high chemoselectivity hinges on an interplay of various minor factors such as the correct positioning of seemingly 'unimportant' second- or third-shell residues constituting proton and electron transfer chains to and from the active site.

Declaration of Competing Interest

The authors declare that they have no known competing financial interests or personal relationships that could have appeared to influence the work reported in this paper.

Acknowledgements

The project was supported by the Ministry of Education, Youth and Sports of the Czech Republic (LTAUSA19148, to L.R. and the EATRIS-CZ program LM2015064, to A.M.) and ERDF/ESF project

"Chemical biology for drugging undruggable targets (ChemBio-Drug)" (No. CZ.02.1.01/0.0/0.0/16_019/0000729).

Appendix A. Supplementary data

Supplementary data to this article can be found online at https://doi.org/10.1016/j.csbj.2022.03.010.

References

[1] Solomon EI, Brunold TC, Davis MI, et al. Geometric and electronic structure/function correlations in non-heme iron enzymes. Chem Rev 2000;100(1):235–349. https://doi.org/10.1021/cr9900275.

[2] Krebs C, Bollinger JM, Booker SJ. Cyanobacterial alkane biosynthesis further expands the catalytic repertoire of the ferritin-like 'di-iron-carboxylate' proteins. Curr Opin Chem Biol 2011;15(2):291–303. https://doi.org/10.1016/j.cbpa.2011.02.019.

[3] Jasniewski AJ, Que L. Dioxygen activation by nonheme diiron enzymes: diverse dioxygen adducts, high-valent intermediates, and related model complexes. Chem Rev 2018;118(5):2554–92. https://doi.org/10.1021/acs.chemrev.7b00457.

[4] Nagai J, Bloch K. Enzymatic desaturation of stearyl acyl carrier protein. J Biol Chem 1968;243(17):4626–33. https://doi.org/10.1016/S0021-9258(18)93235-7.

[5] Morris LJ. Mechanisms and Stereochemistry in Fatty Acid Metabolism - Fifth Colworth Medal Lecture. Biochem J 1970;118(5):681–93. https://doi.org/10.1042/bj1180681g.

[6] Schmidt H, Heinz E. Involvement of ferredoxin in desaturation of lipid-bound oleate in chloroplasts. Plant Physiol 1990;94(1):214–20. https://doi.org/10.1104/pp.94.1.214.

[7] Wada H, Schmidt H, Heinz E, Murata N. *In vitro* ferredoxin-dependent desaturation of fatty-acids in cyanobacterial thylakoid membranes. J Bacteriol 1993;175(2):544–7. https://doi.org/10.1128/jb.175.2.544-547.1993.

[8] Kazaz S, Miray R, Lepiniec L, Baud S. Plant monounsaturated fatty acids: diversity, biosynthesis, functions and uses. Prog Lipid Res 2022;85:. https://doi.org/10.1016/j.plipres.2021.101138101138.

[9] Yang YS, Broadwater JA, Pulver SC, Fox BG, Solomon EI. Circular dichroism and magnetic circular dichroism studies of the reduced binuclear non-heme iron site of stearoyl-ACP Δ^9-desaturase: substrate binding and comparison to ribonucleotide reductase. J Am Chem Soc 1999;121(12):2770–83. https://doi.org/10.1021/ja9822714.

[10] Broadwater JA, Achim C, Munck E, Fox BG. Mössbauer studies of the formation and reactivity of a quasi-stable peroxo intermediate of stearoyl-acyl carrier protein Δ^9-desaturase. Biochemistry-Us 1999;38(38):12197–204. https://doi.org/10.1021/bi9914199.

[11] Siegbahn PEM. Theoretical model studies of the iron dimer complex of MMO and RNR. Inorg Chem 1999;38(12):2880–9. https://doi.org/10.1021/ic981332w.

[12] Fox BG, Lyle KS, Rogge CE. Reactions of the diiron enzyme stearoyl-acyl carrier protein desaturase. Acc Chem Res 2004;37(7):421–9. https://doi.org/10.1021/ar030186h.

[13] Han WG, Noodleman L. Structural model studies for the peroxo intermediate P and the reaction pathway from P -> Q of methane monooxygenase using broken-symmetry density functional calculations. Inorg Chem 2008;47(8):2975–86. https://doi.org/10.1021/ic701194b.

[14] Jensen KP, Bell CB, Clay MD, Solomon EI. Peroxo-type intermediates in class I ribonucleotide reductase and related binuclear non-heme iron enzymes. J Am Chem Soc 2009;131(34):12155–71. https://doi.org/10.1021/ja809983g.

[15] Han WG, Noodleman L. DFT calculations of comparative energetics and ENDOR/Mössbauer properties for two protonation states of the iron dimer cluster of ribonucleotide reductase intermediate X. Dalton T 2009;30:6045–57. https://doi.org/10.1039/b903847g.

[16] Bochevarov AD, Friesner RA, Lippard SJ. Prediction of Fe-57 Mössbauer parameters by density functional theory: a benchmark study. J Chem Theory Comput 2010;6(12):3735–49. https://doi.org/10.1021/ct100398m.

[17] Bochevarov AD, Li JN, Song WJ, Friesner RA, Lippard SJ. Insights into the different dioxygen activation pathways of methane and toluene monooxygenase hydroxylases. J Am Chem Soc 2011;133(19):7384–97. https://doi.org/10.1021/ja110287y.

[18] Han WG, Noodleman L. DFT Calculations for Intermediate and Active States of the Diiron Center with a Tryptophan or Tyrosine Radical in *Escherichia coli* Ribonucleotide Reductase. Inorg Chem 2011;50(6):2302–20. https://doi.org/10.1021/ic1020127.

[19] Srnec M, Rokob TA, Schwartz JK, Kwak Y, Rulisek L, Solomon EI. Structural and Spectroscopic Properties of the Peroxodiferric Intermediate of *Ricinus communis* Soluble Δ^9 Desaturase. Inorg Chem 2012;51(5):2806–20. https://doi.org/10.1021/ic2018067.

[20] Rokob TA. Pathways for Arene Oxidation in Non-Heme Diiron Enzymes: Lessons from Computational Studies on Benzoyl Coenzyme A Epoxidase. J Am Chem Soc 2016;138(44):14623–38. https://doi.org/10.1021/jacs.6b06987.

[21] Chalupský J, Rokob TA, Kurashige Y, et al. Reactivity of the Binuclear Non-Heme Iron Active Site of Δ^9 Desaturase Studied by Large-Scale Multireference *ab initio* Calculations. J Am Chem Soc 2014;136(45):15977–91. https://doi.org/10.1021/ja506934k.

[22] Bím D, Chalupský J, Culka M, Solomon EI, Rulíšek L, Srnec M. Proton-electron transfer to the active site is essential for the reaction mechanism of soluble Δ^9-desaturase. J Am Chem Soc 2020;142(23):10412–23. https://doi.org/10.1021/jacs.0c01786.

[23] Lee M, Lenman M, Banas A, et al. Identification of non-heme diiron proteins that catalyze triple bond and epoxy group formation. Science 1998;280(5365):915–8. https://doi.org/10.1126/science.280.5365.915.

[24] Broun P, Shanklin J, Whittle E, Somerville C. Catalytic plasticity of fatty acid modification enzymes underlying chemical diversity of plant lipids. Science 1998;282(5392):1315–7. https://doi.org/10.1126/science.282.5392.1315.

[25] Cahoon EB, Kinney AJ. Dimorphecolic acid is synthesized by the coordinate activities of two divergent Δ^{12}-oleic acid desaturases. J Biol Chem 2004;279(13):12495–502. https://doi.org/10.1074/jbc.M314329200.

[26] Broadwater JA, Whittle E, Shanklin J. Desaturation and Hydroxylation - Residues 148 and 324 of *Arabidopsis* FAD2, in addition to substrate chain length, exert a major influence in partitioning of catalytic specificity. J Biol Chem 2002;277(18):15613–20. https://doi.org/10.1074/jbc.M200231200.

[27] Robin J, Gueroult M, Cheikhrouhou R, et al. Identification of a crucial amino acid implicated in the hydroxylation/desaturation ratio of *Cp*FAH12 bifunctional hydroxylase. Biotechnol Bioeng 2019;116(10):2451–62. https://doi.org/10.1002/bit.27102.

[28] Behrouzian B, Dawson B, Buist PH, Shanklin J. Oxidation of chiral 9-fluorinated substrates by castor stearoyl-ACP Δ^9 desaturase yields novel products. Chem Commun 2001;8:765–6. https://doi.org/10.1039/b100035g.

[29] Behrouzian B, Savile CK, Dawson B, Buist PH, Shanklin J. Exploring the hydroxylation-dehydrogenation connection: Novel catalytic activity of castor stearoyl-ACP Δ^9 desaturase. J Am Chem Soc 2002;124(13):3277–83. https://doi.org/10.1021/ja012252l.

[30] Rogge CE, Fox BG. Desaturation, chain scission, and register-shift of oxygen-substituted fatty acids during reaction with stearoyl-ACP desaturase. Biochemistry-Us 2002;41(31):10141–8. https://doi.org/10.1021/bi020306d.

[31] White RD, Fox BG. Chain cleavage and sulfoxidation of thiastearoyl-ACP upon reaction with stearoyl-ACP desaturase. Biochemistry-Us 2003;42(25):7828–35. https://doi.org/10.1021/bi030082e.

[32] Whittle EJ, Tremblay AE, Buist PH, Shanklin J. Revealing the catalytic potential of an acyl-ACP desaturase: Tandem selective oxidation of saturated fatty acids. P Natl Acad Sci USA 2008;105(38):14738–43. https://doi.org/10.1073/pnas.0805645105.

[33] Whittle EJ, Cai YH, Keereetaweep J, Chai J, Buist PH, Shanklin J. Castor stearoyl-ACP desaturase can synthesize a vicinal diol by dioxygenase chemistry. Plant Physiol 2020;182(2):730–8. https://doi.org/10.1104/pp.19.01111.

[34] Koo CW, Rosenzweig AC. Biochemistry of aerobic biological methane oxidation. Chem Soc Rev 2021;50(5):3424–36. https://doi.org/10.1039/d0cs01291b.

[35] Wagner S, Klepsch MM, Schlegel S, et al. Tuning *Escherichia coli* for membrane protein overexpression. P Natl Acad Sci USA 2008;105(38):14371–6. https://doi.org/10.1073/pnas.0804090105.

[36] Studier FW. Stable expression clones and auto-induction for protein production in *E. coli*. Methods Mol Biol 2014;1091:17–32. https://doi.org/10.1007/978-1-62703-691-7_2.

[37] Gasteiger E, Hoogland C, Gattiker A, et al. Protein Identification and Analysis Tools on the ExPASy Server. In: Walker JM, editor. The Proteomics Protocols Handbook. Totowa, NJ: Humana Press; 2005. p. 571–607.

[38] Mckeon TA, Stumpf PK. Purification and characterization of the stearoyl-acyl carrier protein desaturase and the acyl-acyl carrier protein thioesterase from maturing seeds of safflower. J Biol Chem 1982;257(20):2141–7. https://doi.org/10.1016/S0021-9258(18)33690-1.

[39] Cahoon EB, Cranmer AM, Shanklin J, Ohlrogge JB. Δ^6 Hexadecenoic Acid Is Synthesized by the Activity of a Soluble Δ^6 Palmitoyl-Acyl Carrier Protein Desaturase in *Thunbergia alata* Endosperm. J Biol Chem 1994;269(44):27519–26. https://doi.org/10.1016/S0021-9258(18)47015-9.

[40] Broadwater JA, Ai JY, Loehr TM, Sanders-Loehr J, Fox BG. Peroxodiferric intermediate of stearoyl-acyl carrier protein Δ^9 desaturase: Oxidase reactivity during single turnover and implications for the mechanism of desaturation. Biochemistry-Us 1998;37(42):14664–71. https://doi.org/10.1021/bi981839i.

[41] Plate M, Overs M, Schafer HJ. Synthesis of enantioenriched methyl *vic*-dihydroxystearates. Synthesis 1998;9:1255–8. https://doi.org/10.1055/s-1998-6084.

[42] Bouchakour M, Daaou M, Duguet N. Synthesis of Imidazoles from Fatty 1,2-Diketones. Eur J Org Chem 2021;2021(11):1647–52. https://doi.org/10.1002/ejoc.202100053.

[43] Frankel EN, Garwood RF, Khambay BPS, Moss GP, Weedon BCL. Stereochemistry of Olefin and Fatty-Acid Oxidation .3. The Allylic Hydroperoxides from the Autoxidation of Methyl Oleate. *J Chem Soc Perk T 1*. 1984(10):2233-2240. doi:10.1039/p19840002233.

[44] Lindqvist Y, Huang WJ, Schneider G, Shanklin J. Crystal structure of Δ^9 stearoyl-acyl carrier protein desaturase from castor seed and its relationship to other di-iron proteins. Embo J 1996;15(16):4081–92. https://doi.org/10.1002/j.1460-2075.1996.tb00783.x.

[45] Jaworski JG, Stumpf PK. Fat-metabolism in higher-plants - properties of soluble stearyl-acyl carrier protein desaturase from maturing *Carthamus tinctorius*. Arch Biochem Biophys 1974;162(1):158–65. https://doi.org/10.1016/0003-9861(74)90114-3.

[46] Kleiman R, Spencer GF. Gas chromatography mass spectrometry of methyl-esters of unsaturated oxygenated fatty-acids. J Am Oil Chem Soc 1973;50 (2):31–8. https://doi.org/10.1007/Bf02886864.
[47] Kishino S, Takeuchi M, Park SB, et al. Polyunsaturated fatty acid saturation by gut lactic acid bacteria affecting host lipid composition. P Natl Acad Sci USA 2013;110(44):17808–13. https://doi.org/10.1073/pnas.1312937110.
[48] Wilson R, Smith R, Wilson P, Shepherd MJ, Riemersma RA. Quantitative gas chromatography mass spectrometry isomer-specific measurement of hydroxy fatty acids in biological samples and food as a marker of lipid peroxidation. Anal Biochem 1997;248(1):76–85. https://doi.org/10.1006/abio.1997.2084.
[49] Xia W, Budge SM. GC-MS characterization of hydroxy fatty acids generated from lipid oxidation in vegetable oils. Eur J Lipid Sci Tech 2018;120 (2):1700313. https://doi.org/10.1002/ejlt.201700313.
[50] Xia W, Budge SM. Simultaneous quantification of epoxy and hydroxy fatty acids as oxidation products of triacylglycerols in edible oils. J Chromatogr A 2018;1537:83–90. https://doi.org/10.1016/j.chroma.2017.12.066.
[51] Sobrado P, Lyle KS, Kaul SP, et al. Identification of the binding region of the [2Fe-2S] ferredoxin in stearoyl-acyl carrier protein desaturase: Insight into the catalytic complex and mechanism of action. Biochemistry-Us 2006;45 (15):4848–58. https://doi.org/10.1021/bi0600547.